IL NUOVO CIMENTO **45 C** (2022) 66
DOI 10.1393/ncc/i2022-22066-y

COMMUNICATIONS: SIF Congress 2021

Testing three-body forces in the oxygen region via lifetime measurements

I. ZANON(1)(2)

(1) *Laboratori Nazionali di Legnaro - Legnaro, Italy*
(2) *Dipartimento di Fisica e Scienze della Terra, Università degli Studi di Ferrara - Ferrara, Italy*

received 31 January 2022

Summary. — The ^{20}O nucleus represents an interesting case of study. In this nucleus, the spectroscopic properties of the 2_2^+ and 3_1^+ states are influenced by the contribution of three-body forces. Hence, lifetime measurements of these states can provide meaningful information on the role of three-body forces in this nucleus. An experiment aimed at measuring the lifetime of 2_2^+ and 3_1^+ states of ^{20}O using the Doppler Shift Attenuation method was performed at GANIL, using the AGATA array coupled to the MUGAST array and the VAMOS++ spectrometer. The lifetimes of the states were extracted by comparing the experimental data to Monte Carlo simulations. In this paper, the spectroscopic study of the ^{20}O via particle-γ coincidences is presented.

1. – Introduction

Three-body (3N) forces are key elements in the study of nuclear structure and, in particular, in the evolution of the nuclear interaction from the valley of stability toward more exotic nuclei. The effect of these forces have been observed in different regions of the Segré chart, in light-mass (such as in the case of ^{4}He, ^{10}Be, ^{13}C and the oxygen isotopic chains [1]), medium-mass (^{22}Na and ^{46}V [2]) and heavy-mass nuclei (tin isotopes [3]). The 3N forces can affect the bulk properties of the nucleus, such as the radii and the binding energies, but also spectroscopic properties such as excitation energies and lifetimes of the states as well as electroweak transitions [4].

In this context, the oxygen isotopic chain represents a peculiar case. In this region, the neutron drip line follows a regular pattern, with the exception of the oxygen chain. According to shell-model calculations, the neutron drip line is expected to be on ^{28}O. This isotope corresponds to $N = 20$ and, having $Z = 8$, is expected to be a doubly-magic nucleus, corresponding to the neutron *sd*-shell closure. However, experiments have proven that the ^{26}O and ^{28}O nuclei decay via neutron emission, moving the drip line to ^{24}O, corresponding to $N = 16$ [1].

The correct neutron drip line has been reproduced in the work of Otsuka *et al.* [5], where 3N forces were introduced into the calculations. These forces have the effect of raising the single particle energies of the $s_{1/2}$ and $d_{3/2}$ orbitals, in particular moving the latter one to positive values, hence changing the drip line from the filling of the $d_{3/2}$ orbital to the $s_{1/2}$ orbital. This study proved the importance of 3N forces in the calculation of the nuclear interaction in this region. However, additional information is needed to quantify their contribution.

Due to experimental difficulties, not all oxygen isotopes and not all observables are easily accessible for measurements. In this context, the ^{20}O nucleus represents an interesting case. Being close to the stable ^{18}O isotope, the ^{20}O has been studied since the Seventies using different reaction mechanisms. In particular, by using a (t, p) reaction starting from a triton beam impinging on a ^{18}O target, the excitation energies and angular distributions of the low-lying states were investigated [6]. In this work, by comparing the results with shell-model calculations, the nature of these states was determined: the positive-parity states were attributed to a $(sd)^4$ and $(sd)^6(1p)^{-2}$ character; on the other hand, negative states were attributed to a mixing of $(sd)^5(1p)^{-1}$ and $(sd)^3(fp)^1$ configurations.

Of the positive-parity states, the $0^+_{\text{g.s.}}$, 2^+_1 and 4^+_1 are based on a pure neutron $\nu(d_{5/2})^4$ configuration, while the 2^+_2 and the 3^+_1 states are based on a configuration of $\nu(d_{5/2})^3(s_{1/2})^1$. The 2^+_2 and 3^+_1 states are sensitive to the relative positions of the *sd*-shell orbitals. Lowering the $d_{3/2}$ orbital, in particular, makes it compete with the $d_{5/2}$ and $s_{1/2}$ orbitals. Therefore, properties of these two states are expected to be sensitive to 3N forces.

Ab initio calculations employing the Many Body Perturbation Theory (MBPT) [7] proved that the contribution of 3N forces affects the lifetime of these states: when 3N forces are neglected in the framework, the lifetime of the 2^+_2 state increases by $\sim$60%. These results suggest that it is possible to put constraints on the influence of 3N forces in the nuclear interaction in this region by measuring the lifetime of these states.

In a previous experiment [4], employing transfer and deep-inelastic reactions starting from a beam of ^{18}O and a target of ^{181}Ta, the lifetime of the 2^+_2 state was measured ($\tau = 150^{+80}_{-30}$ fs).

A new experiment, using a different reaction mechanism, was performed in 2020. The goal of this experiment was to re-measure the lifetime of the 2^+_2 state and to measure the one of the 3^+_1 for the first time. The details of the experiment are presented in sect. **2**. The preliminary results of the spectroscopic study of the ^{20}O nucleus are presented in sect. **3**.

2. – Experimental details

Direct reactions are powerful tools to study the structure of nuclei and (d, p) reactions in particular can provide meaningful information on the single-particle states of the nucleus by means of angular distributions and cross sections. For the present experiment, a (d, p) reaction was chosen because it has been observed [8] to favor the population of the states of interest with respect to other states. Moreover, as it will be presented in the next section, (d, p) reactions allow for a control on the direct population of the states.

The ^{20}O was populated using a radioactive ion beam of ^{19}O impinging on a deuterated polyethylene (CD_2) target. The beam was provided by the SPIRAL1 complex [9] of GANIL and post-accelerated to a beam energy of 8 MeV/A, while the average intensity

of the current was 4×10^5 pps. The beam purity was analysed in search of contaminants but no other isotopes than ^{19}O were found. The target composition was also analysed using a scanning electron microscope. The measured thickness was $300\,\mu g/cm^2$; however, some inhomogeneity was observed due to the presence of bubbles. Two different types of target were prepared: a self-supporting CD_2 target, employed for a spectroscopic study of the ^{20}O, and a CD_2 target deposited on a $20\,mg/cm^2$ layer of ^{nat}Au. This second target was employed to perform lifetime measurements of the states using the Doppler-shift Attenuation Method (DSAM) [10].

Due to the reaction dynamics, the ^{20}O recoils were emitted in a forward cone with an angular opening of less than 6°. The magnetic spectrometer VAMOS++ [11] was placed at forward angles (see fig. 1). Due to their similarity in mass, it was not possible to exclude the residual beam from the angular acceptance of the spectrometer, leading to a counting rate in the spectrometer of the order of the beam current. At these counting rates, the drift and ionization chambers result to be inefficient due to pile-up effects. For this reason, only the Multi-Wire Parallel Avalance Counter (MWPAC) of VAMOS, placed after the dipole, was employed. The magnetic rigidity Bρ of the dipole was set in correspondence of the ^{20}O recoil and a Time-of-Flight (ToF) measurement was performed in order to distinguish between the even of interest and the background events coming from the elastic scattering of the beam or the fusion-evaporation residues.

At backward angles with respect to the beamline, the array of silicon detectors MUGAST [12] was placed (see fig. 1), in order to detect the protons emitted in the reaction. Thanks to the high-segmentation of the detectors, a good energy and angular resolution was obtained. In particular, from the information obtained from the protons, it was possible to reconstruct the kinematics of the reaction and hence obtain the velocity vector and the excitation energy of the ^{20}O nucleus. Finally, γ rays were detected using the AGATA array [13], placed at backward angles. The AGATA array, which at the moment

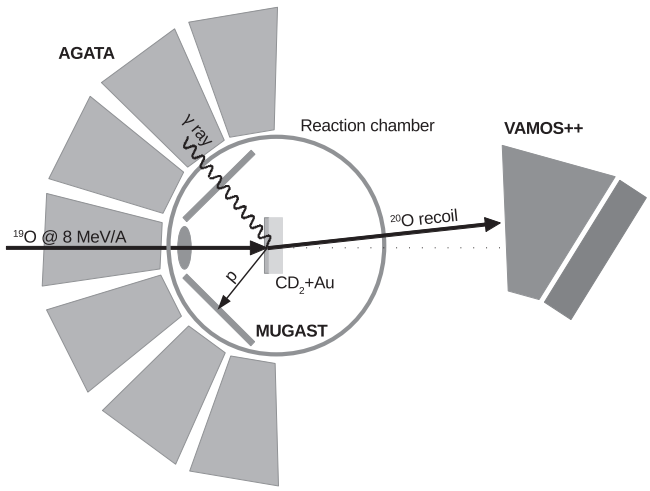

Fig. 1. – Scheme of the experimental setup. At backward angles with respect to the beam direction, the AGATA spectrometer is placed. Inside the reaction chamber, at backward angles, the trapezoidal and annular silicon detectors of the MUGAST array are placed, as well as the CD_2 target deposited on the gold degrader. The beam-like recoil, ^{20}O, is emitted at forward angles and detected by the VAMOS++ spectrometer. The different arrays are not in scale.

of the experiment counted 36 detectors, constitutes the state-of-the-art of germanium detectors. Thanks to the high-segmentation of the crystals and the tracking algorithm, coupled to the Pulse Shape Analysis (PSA) technology, this array allows a good energy and angular resolution. The combined capabilities of AGATA and MUGAST ensure a good Doppler correction (DC), which is fundamental for an analysis based on the line-shape of the peak, such as lifetime measurements using the DSAM. More details about the kinematic reconstruction and the event-by-event Doppler correction events can be found in refs. [12, 14, 15].

3. – Spectroscopic analysis

From the kinematic reconstruction obtained from the detection of the protons, it was possible to reconstruct the excitation energy spectrum of the ^{20}O, presented in fig. 2. The spectrum has been obtained by selecting the events expected in coincidence with the ^{20}O ions, by applying a time gate between VAMOS and MUGAST and between VAMOS and the cyclotron radiofrequency. A good energy resolution, with a Full Width Half Maximum (FWHM) of 179 keV for the peak at 1.7 MeV [12], allowed for a clear identification of the most intense peaks. In particular, one can observe the ground state peak, the 2^+_1 at 1.7 MeV, the 4^+_1 at 3.5 MeV, the 2^+_2 at 4.1 MeV and the 3^+_1 state at 5.2 MeV. Moreover, it allowed for the discrimination of other, less populated, excited states, as the one around 5.0 MeV and the one around 5.6 MeV. These two states have been observed also by Hoffman *et al.* [8], that assigned them a tentative spin and parity of 2^+. This experiment exploited the same (d, p) reaction at a similar beam energy (6.61(3) MeV/u) and with a similar target thickness (260 μg/cm^2), employing HELIOS [16]. A FWHM of 175 keV was measured in the excitation energy spectrum, similar to the conditions obtained in the present experiment. The MUGAST array allows for the retrieving of the selectivity and resolution of setups like HELIOS, and additionally its compact configuration allows one to couple it to γ-ray spectrometers such as AGATA to perform γ-particle coincidence analyses.

By gating on the excitation energy spectrum, it was possible to study the γ-particle coincidences and reconstruct the level scheme of the nucleus of interest. For this procedure,

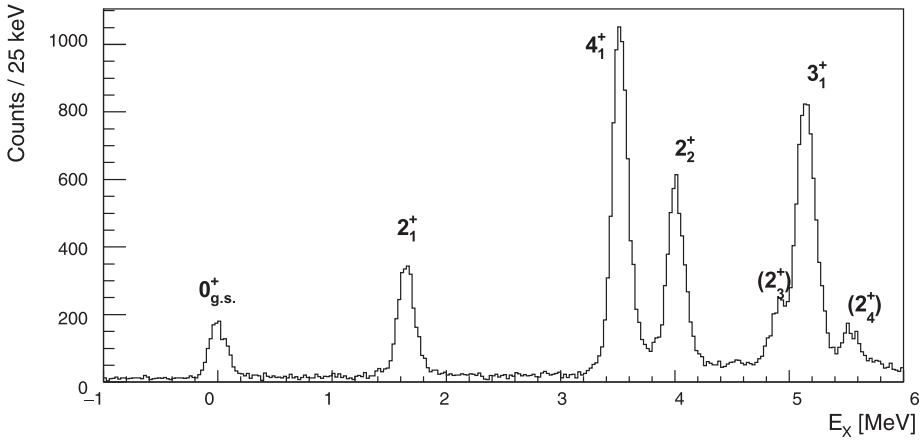

Fig. 2. – Reconstructed excitation energy spectrum of the ^{20}O nucleus obtained from information of the protons detected by the MUGAST array at backward angles.

the data set employing the CD_2-only target was employed. In this data set, the γ-ray transitions are not affected by the Doppler shift caused by the energy loss in the degrader, as in the case of the data set using the CD_2 + Au target.

Figure 3 shows the γ-ray spectra obtained with four different particle gates on the excitation energy spectrum. The double gate on the time coincidence and the ^{20}O excitation energy guarantees an extremely clean spectrum with low background.

The first spectrum (fig. 3(a)) was obtained by requiring an energy gate between 1.55 and 1.95 MeV, in correspondence to the 2_1^+ state. As expected, only one transition, corresponding to the $2_1^+ \rightarrow 0^+_{\text{g.s.}}$, is observed at 1674.5(4) keV. This value is in agreement with previous measurements [4, 17].

The second spectrum (fig. 3(b)) was obtained by requiring an energy gate between 3.35 and 3.75 MeV, in correspondence to the 4_1^+ state. The $2_1^+ \rightarrow 0^+_{\text{g.s.}}$ is observed at 1674.2(3) keV, confirming the previous measurement. A second transition, corresponding to $4_1^+ \rightarrow 2_1^+$, is also observed at 1897.7(3) keV. These two measurements place the 4_1^+ state at 3571.9(9 keV, which is in agreement with the excited state reconstructed by MUGAST.

The third spectrum (fig. 3(c)) was obtained by requiring an energy gate between 3.95 and 4.35 MeV, in correspondence to the 2_2^+ state. The $2_1^+ \rightarrow 0^+_{\text{g.s.}}$ transition was observed at the same energy as in the previous cases. The 2_2^+ state was observed to decay via two transitions: the $2_2^+ \rightarrow 2_1^+$ transition at 2396.0(4) keV and the $2_2^+ \rightarrow 0^+_{\text{g.s.}}$ at 4071(1) keV. When summing the energies of the $2_2^+ \rightarrow 2_1^+$ and $2_1^+ \rightarrow 0^+_{\text{g.s.}}$ transitions, one obtains 4071(1) keV, which is compatible with the measurement of the $2_2^+ \rightarrow 0^+_{\text{g.s.}}$ energy transition and the measurement obtained with MUGAST for the 2_2^+ state. The absence of the $4_1^+ \rightarrow 2_1^+$ transition around 1898 keV in the spectrum is a confirmation of the selectivity of the energy gate.

Finally, the fourth spectrum (fig. 3(d)) was obtained by requiring an energy gate between 5.10 and 5.50 MeV, in correspondence to the 3_1^+ state. In the spectrum, one can immediately identify the $2_1^+ \rightarrow 0^+_{\text{g.s.}}$ transition at the expected energy, as well as the $2_2^+ \rightarrow 2_1^+$ transition at 2397(1) keV. This means that one branching from the 3_1^+ state is expected to decay to the 2_2^+ state. This is confirmed by the observation of a transition at 1156.0(8) keV, that summed to the excitation energy of 2_2^+, is compatible with the excitation energy of the 3_1^+ state. The second, more intense, branching is observed at 3552.6(6) keV and is attributed to the $3_1^+ \rightarrow 2_1^+$ transition.

The presence of the first branching is particularly important for the present analysis. In fact, the population of the 2_2^+ state due to the decay of the 3_1^+ state, rather than to the direct population at reaction point, may influence the lifetime measurement of the 2_2^+ in case the 3_1^+ state has a comparable or longer lifetime. In particular, if the feeding from the 3_1^+ is not taken into account, it will lead to a systematic error pointing to longer lifetimes. For this reason, the possibility of selecting events corresponding to the direct population of the state by gating on the excitation energy spectrum of MUGAST (as per fig. 3(c)), is crucial for this analysis, as it allows for the exclusion of the feeders contribution.

As for the states at 5.0 and 5.6 MeV, the statistics collected with the CD_2-only target are not sufficient for the analysis. The dataset using the CD_2 + Au target, instead, presents higher statistics. Despite the Doppler-shift effects due to the energy loss in the degrader, it is still possible to study the transitions decaying from the selected states. For this, two different event-by-event Doppler correction must be introduced. The first one is achieved by using the velocity vector of the ^{20}O recoil reconstructed using the protons

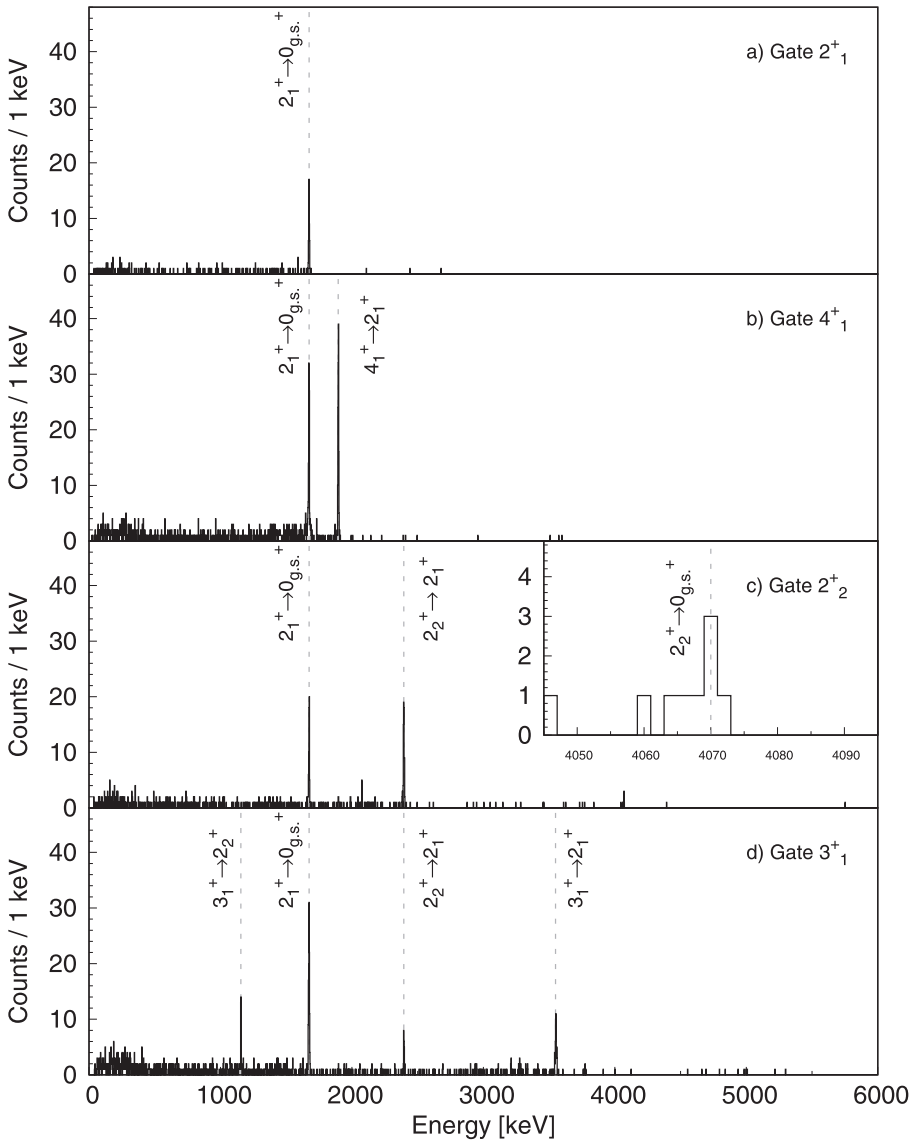

Fig. 3. – γ-ray energy spectra with different gates on the excitation energy of ^{20}O in correspondence to the excited states 2^+_1 (a), 4^+_1 (b), 2^+_2 (c) and 3^+_1 (d). The identified transitions are highlighted (dashed grey line).

detected by MUGAST at backward angles. As the protons are emitted at the reaction point, this Doppler correction does not consider the energy loss in the degrader and it is referred to as *fast DC*. The second one is obtained from the first one by calculating the energy loss of the ^{20}O recoil in the gold degrader, taking into account the angle of emission and hence the effective thickness of the target. It is referred to as *slow DC*. The spectra obtained with the two Doppler corrections and the two different gates are presented in fig. 4.

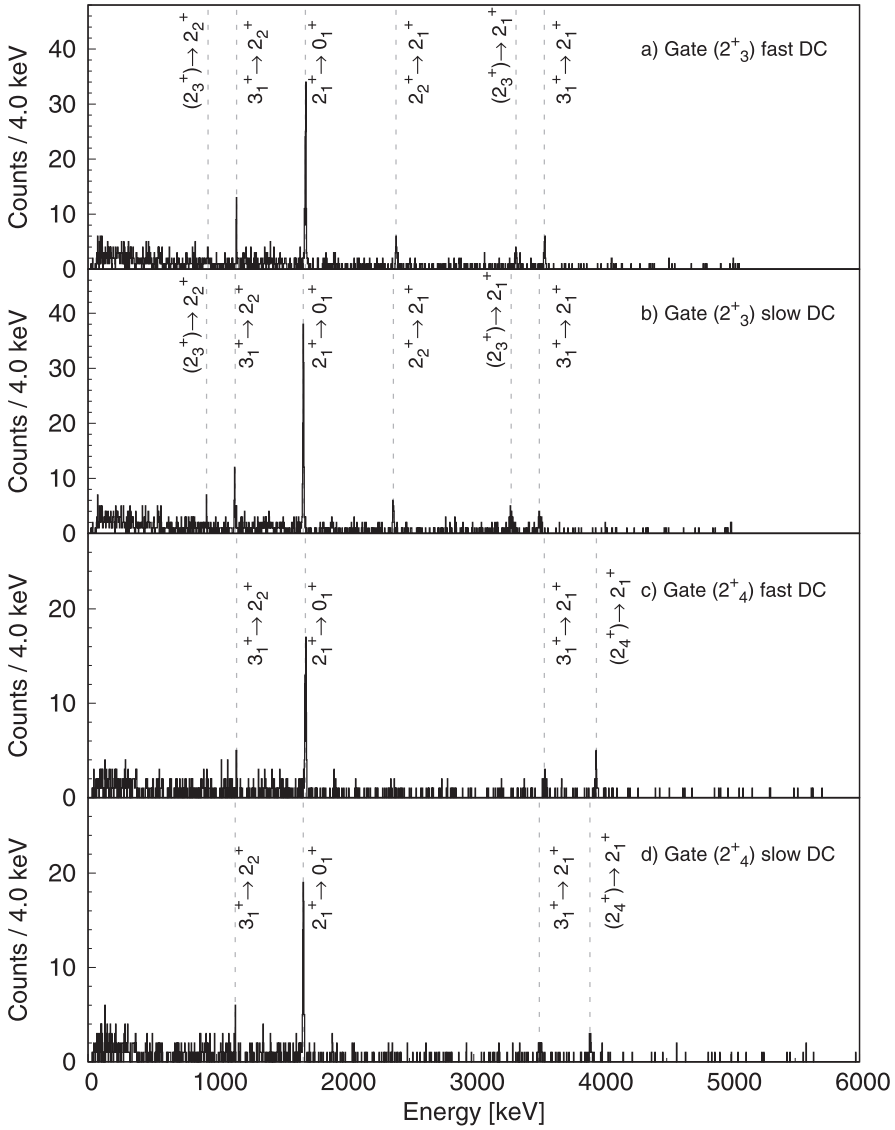

Fig. 4. – γ-ray energy spectra with different gates on the excitation energy of ^{20}O in correspondence to the excited states (2^+_3) with fast DC (a) and slow DC (b), and (2^+_4) with fast DC (c) and slow DC (d). The identified transitions are highlighted (dashed grey line).

The gate on the 5.0 MeV is taken from 4.75 to 5.15 MeV. Being too close to the 3^+_1 state, it is impossible to gate on the (2^+_3) state without partially including contamination from this state. In fact, it is possible to observe both the $3^+_1 \to 2^+_1$ transition around 3.5 MeV and the $3^+_1 \to 2^+_2$ transition around 1.2 MeV. Despite the low statistic it is possible to notice a peak at 3329(2) keV (fast DC), and its counterpart at 3291(5) keV in the slow DC spectrum. This transition may correspond to the $(2^+_3) \to 2^+_1$. Summing the measured transition energies with the excitation energy of the 2^+_1 places the (2^+_3) state at 5003(2) keV in the first case (*i.e.*, in case the correct energy is found in the fast DC) and 4965(5) keV in the second case (slow DC). Both measurements are compatible

to the MUGAST measurement of the excited state, hence the observed transition can be attributed to the $(2_3^+) \rightarrow 2_1^+$. Another transition is observed around 0.9 MeV. In particular, it is measured at 933(2) keV in the fast DC spectrum and at 922(2) keV in the slow DC spectrum. This transition may correspond to the $(2_3^+) \rightarrow 2_2^+$ transition, placing the (2_3^+) state at 5004(2) keV in the first case and 4493(2) in the second case, both compatible with the MUGAST measurement within the sensitivity of the detectors. The first case is also compatible to the measurement of the (2_3^+) excitation energy obtained with the $(2_3^+) \rightarrow 2_1^+$ transition in the fast DC. Hence, it is possible to conclude that the correct energies of the $(2_3^+) \rightarrow 2_1^+$ and $(2_3^+) \rightarrow 2_2^+$ transitions are 3329(2) keV and 933(2) keV respectively. Finally, in the spectra one can identify the $2_2^+ \rightarrow 2_1^+$ and $2_1^+ \rightarrow 0_{\text{g.s.}}^+$ transitions. These transitions come from the decay of the 3_1^+ and the (2_3^+) states to lower-energy states.

The gate on the 5.6 MeV is taken from 5.45 to 5.85 MeV. Similarly to the previous case, being too close to the 3_1^+ state, it is possible to observe the transitions coming from the depopulation of that state. It is possible to observe a transition at 3954(5) keV (fast DC) and its counterpart at 3903(3) keV (slow DC). This transition may correspond to the $(2_4^+) \rightarrow 2_1^+$. Summing the transition energy to the excitation energy of the 2_1^+ one obtains 5628(5) keV in the first case and 5577(5) keV in the second case. Both scenarios are compatible to the measurement of MUGAST and the results of ref. [8] within the experimental uncertainties. No other branches have been observed. The reconstructed level scheme with the transitions observed in the present experiment is presented in fig. 5. The width of the arrows represents the intensity of the transitions.

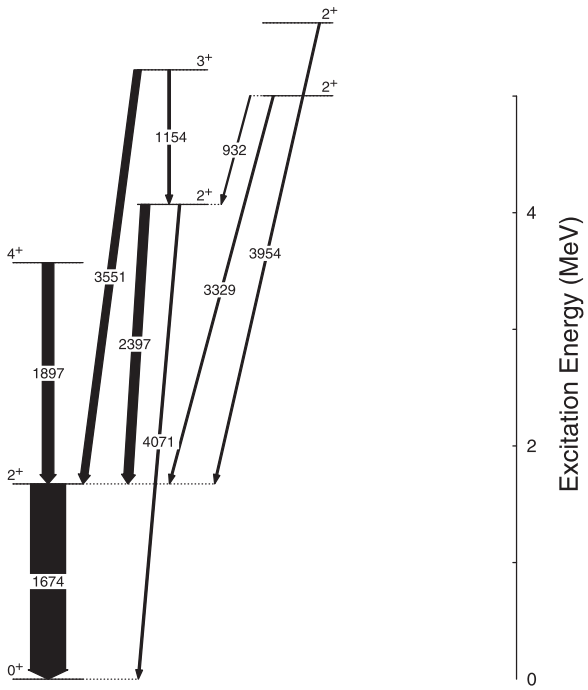

Fig. 5. – Reconstructed level scheme of the ^{20}O nucleus. The arrows width is proportional to the intensity of the transitions.

4. – Conclusions and future perspective

In this experiment, the powerful capabilities of AGATA and MUGAST have been proven. In particular, the thin target and the good angular resolution of the silicon detectors of MUGAST allowed for the kinematic reconstruction of the ^{20}O recoil. This information was employed both for the event-by-event Doppler correction and for the reconstruction of the excitation energy spectrum. Seven excited states of ^{20}O were identified. By selecting on the direct populations of these states it was possible to study the γ-ray transitions decaying from these levels and reconstruct the level scheme of the nucleus. The energy and angular resolutions of AGATA, combined with the Doppler correction, allowed for a precise measurement of the transition energies that resulted compatible with previous measurements within the experimental uncertainties. Four γ-ray transitions were observed for the first time: the $3^+_1 \rightarrow 2^+_2$, $(2^+_3) \rightarrow 2^+_1$, $(2^+_3) \rightarrow 2^+_2$ and $(2^+_4) \rightarrow 2^+_1$ transitions. The two transitions decaying to the 2^+_2 states are particularly interesting for the present experiment. In fact, by populating this state indirectly, they influence the lifetime measurement of the 2^+_2 and must be taken into account when performing the line-shape analysis. However, as shown in the present paper, the powerful capabilities of MUGAST allow one to select the direct population of the state of interest, hence eliminating the contributions from the feeders.

The natural continuation of this analysis is the lifetime measurement of the 2^+_2 and 3^+_1 states which, from the preliminary observations and theoretical predictions, are expected in the range of sensitivity of the DSAM. Additionally, the experimental results will be compared to theoretical calculations.

The study of the influence of 3N forces was extended to the carbon isotopic chain, and in particular to the ^{16}C. This nucleus presents a structure similar to ^{20}O. An experiment devoted to study the lifetime of the first 2^+_1 state using the plunger technique measured this state at an excitation energy of 1762 keV and with a lifetime of 11.4(9) ps [18], in agreement with No-Core Shell-Model (NCSM) predictions [19]. In the same work, a second 2^+ state was also observed at 3979 keV. The $2^+_2 \rightarrow 2^+_1$ transition was observed to decay rapidly, below the range of sensitivity of the plunger. A 3^+_1 state was also observed at 4079 keV, decaying to 2^+_1 with a 2317- keV γ-ray transition. Due to the low statistics, it was not possible to draw conclusions on the lifetime of the state.

NCSM calculations [19] were performed employing two-body and three-body interactions. It was observed that the strong suppression of the $2^+_2 \rightarrow 0^+_{\text{g.s.}}$ transition (branching ratio <8.8% [18]) was well reproduced by the theoretical calculations that included 3N forces. These same calculations emphasized the strong sensitivity of the 3^+_1 state lifetime to the contribution of 3N forces.

For these reasons, an experiment devoted to measuring the lifetimes of the 2^+_2 and 3^+_1 states of ^{16}C using DSAM was proposed and performed by the same collaboration, choosing a setup and a reaction similar to the ^{20}O experiment. The nucleus of interest was populated in a (d, p) reaction starting from a radioactive beam of ^{15}C at 8.2 MeV/A, provided by the RAISOR facility at the Argonne National Laboratory. The beam impinged on a CD_2 target evaporated on a $^{\text{nat}}$Au degrader, employed to slow down the ^{16}C recoil. This reaction was based on a similar experiment performed in ANL using HELIOS [20]. The protons emitted in the reaction were detected using the ORRUBA silicon array [21], coupled to GRETINA [22] for the detection of γ rays. The analysis of this experiment is still on-going, however, from preliminary observations, the 2^+_2 and 3^+_1 states appear to be in the range of sensitivity for the lifetime measurements using DSAM.

The results of these two experiments, compared to theoretical calculations, will allow for a more complete picture of the influence of three body forces in this region.

* * *

The author would like to acknowledge the work of E. Clément, A. Goasduff and M. Ciemała. The author would also like to thank the AGATA, MUGAST and VAMOS++ Collaborations. CloudVeneto is acknowledged for the use of computing and storage facilities.

REFERENCES

[1] Hebeler K. *et al.*, *Annu. Rev. Nucl. Part. Sci.*, **65** (2015) 457.
[2] Hammer H.-W. *et al.*, *Rev. Mod. Phys.*, **85** (2013) 197.
[3] Morris T. D. *et al.*, *Phys. Rev. Lett.*, **120** (2018) 152503.
[4] Ciemała M. *et al.*, *Phys. Rev. C*, **101** (2020) 021303(R).
[5] Otsuka T. *et al.*, *Phys. Rev. Lett.*, **105** (2010) 032501.
[6] LaFrance S. *et al.*, *Phys. Rev. C*, **20** (1979) 1673.
[7] Entem D. R. and Machleidt R., *Phys. Rev. C*, **68** (2003) 041001(R).
[8] Hoffman C. R. *et al.*, *Phys. Rev. C*, **85** (2012) 054318.
[9] Delahaye P. *et al.*, *Nucl. Instrum. Methods. B*, **463** (2020) 339.
[10] Devons S. *et al.*, *Proc. Phys. Soc.*, **68** (1955) 18.
[11] Rejmund M. *et al.*, *Nucl. Instrum. Methods A*, **646** (2010) 184.
[12] Assié M. *et al.*, *Nucl. Instrum. Methods A*, **1014** (2021) 165743.
[13] Akkoyun S. *et al.*, *Nucl. Instrum. Methods A*, **668** (2012) 26.
[14] Zanon I., *Nuovo Cimento C*, **044** (2021) 83.
[15] Zanon I., PhD Thesis (2021).
[16] Lighthall J. *et al.*, *Nucl. Instrum. Methods A*, **622** (2010) 97.
[17] Wiedeking M. *et al.*, *Phys. Rev. Lett*, **94** (2005) 132501.
[18] Petri M. *et al.*, *Phys. Rev. C*, **86** (2012) 044329.
[19] Forssén C. *et al.*, *J. Phys. G*, **40** (2013) 055105.
[20] Wuosmaa A. H. *et al.*, *Phys. Rev. Lett.*, **105** (2010) 132501.
[21] Pain S. *et al.*, *AIP Conf. Proc.*, **1090** (2009) 570.
[22] Lee I. *et al.*, *Nucl. Phys. A*, **746** (2004) 255.